Deformation and Alignment of Lamellae in Melt Extension of Blends of a Styrene-Butadiene Block Copolymer with Polystyrene

Ulrich A. Handge,[1]* Matthias Buschnakowski,[2] Goerg H. Michler[2]

[1]*Department of Materials, Polymer Physics, ETH Zurich, Wolfgang-Pauli-Strasse 10, 8093 Zurich, Switzerland*
[2]*Department of Physics, Martin-Luther-University Halle-Wittenberg, 06099 Halle/S, Germany*

Received 11 May 2008; accepted 2 November 2008
DOI 10.1002/app.29601
Published online 30 January 2009 in Wiley InterScience (www.interscience.wiley.com).

ABSTRACT: The development of the morphology and the alignment of lamellae in melt elongation of blends of an asymmetric linear styrene-butadiene block copolymer (LN3) and polystyrene (PS 158K) was investigated. PS 158K and LN3 formed two-phase polymer blends with PS 158K resp. LN3 inclusions, depending on the concentration of polystyrene. The block copolymer was arranged in a lamellar phase with a lamellae thickness of $\sim$ 13 nm. Our rheological experiments revealed that the complex modulus, the elongational viscosity and the recovered stretch of the blends primarily resulted from a superposition of the properties of the blend components. In melt elongation, pure LN3 started to crumple at a small Hencky strain. In the blends, the presence of the PS 158K inclusions led to a macroscopically more uniform elongation, but with an anisotropic Poisson ratio. The LN3 inclusions in the PS 158K matrix were deformed into a filament-like shape. In the blends with a LN3 matrix the alignment of the block copolymer lamellae parallel to the loading direction increased with applied extensional strain. In the latter case, the lamellae thickness did not decrease significantly.
 J Appl Polym Sci 112: 1319–1329, 2009

Key words: block copolymers; rheology; polymer blends; microphase separation

INTRODUCTION

The variety of applications of block copolymers is associated with their large number of equilibrium and nonequilibrium microstructures.[1–5] By modifying the molecular architecture, the morphology of block copolymers in the microphase-separated state can be controlled and their macroscopic properties can be tailored over a wide range. For example, the combination of a stiff and a soft phase in styrene-butadiene block copolymers has become a successful approach to achieve attractive end-use properties.[6] Blending a block copolymer with a general purpose polystyrene can lead to nanostructured materials with favorable properties by maintaining reasonable costs. Consequently, blends of block copolymers and a homopolymer belong to a technologically highly important class of materials, and their mechanical and rheological properties are intensively studied.[7–11]

Since processing of polymers is intimately related to the melt rheology in shear and elongation, a series of studies investigated the flow behavior and the deformation of pure block copolymers and related blend systems.[12–20] Besides the knowledge of the shear and extensional viscosity, additional elongational properties such as strain-hardening and melt stability are of interest for technological applications. The alignment of lamellae in shear were the subject of several studies, see, e.g., Ref. 21 for a review. Linear viscoelastic shear oscillations of block copolymers with a lamellar morphology were frequently performed.[22,23] Kawasaki and Onuki[24] theoretically explained the characteristic power laws $G' \approx G'' \propto \omega^{1/2}$ for a lamellar morphology. Qiao et al.[25] studied the contraction of lamellae under shear for a diblock copolymer (styrene-ethylene propylene) melt. Their analysis revealed that the relative lamellar spacing was a function of the macroscopic shear stress. The influence of the molecular architecture of several styrene-butadiene triblock copolymers with similar styrene and butadiene content was investigated by Thunga et al.[26] The dynamics of kink bands in a shear field was determined using electron microscopy and small angle X-ray scattering in Refs. 17,18. The work of Geiger et al. was devoted to the rheology of triblock

**Present address:* Department of Polymer Engineering - FAN A.2.04, University of Bayreuth, Universitätsstrasse 30, 95447 Bayreuth, Germany.
Correspondence to: U. A. Handge (ulrich.handge@uni-bayreuth.de).
Contract grant sponsors: Government of Sachsen-Anhalt, German Science Foundation, Kultusministerium des Landes Sachsen-Anhalt.

copolymers under extrusion conditions. In addition, the order parameter was determined by measuring the form birefringence and by performing X-ray scattering experiments. Leist et al.[28] investigated the orientation flip of lamellar polystyrene-polyisoprene diblock copolymers under extrusion conditions and showed that parallel and perpendicular orientations can be obtained. The surface characteristics of triblock and pentablock copolymers after extrusion were also investigated.[29,30] Finally, Fourier transformation rheology was applied to detect the microphase reorientation in block copolymer melts and the flip of lamellae in shear flows.[31,32]

Melt extension experiments of several block copolymer melts were performed by Takahashi et al.,[33] Kotaka et al.,[34] and Kobori et al.[35] Takahashi et al.[33] studied the nonlinear properties of a poly(styrene-*block*-butadiene-*block*-styrene) melt in shear and elongation. The extensional properties of a blend of polystyrene-*block*-poly(ethylene butylene)-*block*-polystyrene and polystyrene with cylindrical domains were determined for domains which were aligned parallel and perpendicular to the loading direction.[35] Lee et al.[36] studied the rheological properties of a styrene-isoprene-styrene triblock copolymer in shear and elongation and characterized the morphology for parallel and perpendicular orientation.

The thermodynamical, mechanical, and rheological properties of blends of a block copolymer and a homopolymer were the subject of several studies. Nojima and Roe[37] investigated the influence of polystyrene on the order-disorder temperature of styrene-butadiene diblock copolymers and reported a good agreement between experimental data and the theoretical prediction based on the random phase approximation. The influence of the extrusion properties such as temperature and shear rate on the morphology and micromechanical properties of blends of styrene-butadiene star block copolymer and commercial polystyrene was studied in Ref. 38. This study demonstrates that the blend morphology strongly influences the mechanical properties. Finally, a systematic study on the rheological and mechanical properties of blends of a polystyrene-polyisobutylene-polystyrene triblock copolymer and polystyrene was performed by Antony et al.[39] to determine the optimum blend composition.

In this work, we investigated the rheology of molten blends of polystyrene (PS 158K) and a styrene-butadiene block copolymer (LN3) in homogeneous shear and extensional flows. The overall content of styrene in the block copolymer was 74%. This large styrene content usually leads to a spherical morphology. Because of its asymmetric molecular architecture, the block copolymer was arranged in a lamellar phase.[40] Depending on the concentration of the polystyrene PS 158K phase, the styrene-butadiene block copolymer formed inclusions or a continuous matrix. We explored the microscopic deformation and alignment of the lamellar phase during elongation and after subsequent relaxation and recovery. Our focus was the deformation to a large stretch ratio. In the LN3-rich systems, the macroscopic extension was applied to the LN3 matrix, whereas in the case of a PS 158K matrix, small LN3 inclusions with a few lamellae were deformed by the surrounding PS 158K matrix. The objective of our work was to gain insight into the dynamical deformation, relaxation and recovery behavior of the lamellar phase.

EXPERIMENTAL

Materials

The components of the blends were polystyrene PS 158K and the styrene-butadiene block copolymer LN3. Both materials were supplied by BASF SE (Ludwigshafen, Germany). PS 158K is a polydisperse homopolymer with $M_w/M_n = 3.10$, see Table I. LN3 is an asymmetric linear block copolymer which consists of two outer styrene blocks of different lengths. The middle part between these two styrene blocks is composed of two random styrene-butadiene blocks with different ratios of styrene and butadiene. The molecular architecture of LN3 is schematically shown in Figure 1. LN3 was synthesized by anionic living polymerization using butyllithium as initiator in cyclohexane as solvent.[6] The overall content of polystyrene in LN3 is 74%.[40] Because of the asymmetric structure, the block copolymer chains were arranged in lamellae, see also Ref. 40 for a detailed discussion of the morphology of symmetric and asymmetric styrene-butadiene block copolymers.

TABLE I
Glass Transition Temperature T_g (Determined by Differential Scanning Calorimetry), Number and Weight Average M_n and M_w of the Molecular Weight and Density ρ of Polystyrene PS 158K and the Styrene-Butadiene Block Copolymer LN3 (BASF SE, Ludwigshafen, Germany)

	$T_{g,\mathrm{PS}}$ (°C)	$T_{g,\mathrm{soft}}$ (°C)	Total content of PS (%)	M_n (g/mol)	M_w (g/mol)	M_w/M_n	ρ at 25°C (g/cm^3)	ρ at 170°C (g/cm^3)
PS 158K	105	–	100	96 600	299 000	3.10	1.050	0.983
LN3	102	−50	74	127 300	140 000	1.10	1.010	0.931

The data for LN3 are taken from Ref. 40 and the density for PS 158K is taken from Ref. 41.

Figure 1 Scheme of the molecular architecture of the styrene-butadiene copolymer LN3 used in this study. This block copolymer is composed of two outer PS blocks (in gray color) which surround two random styrene-butadiene blocks (soft phase, in hatched style).

Three blends of PS 158K and LN3 were prepared with different weight fractions Φ_{PS} of the PS 158K phase, i.e., $\Phi_{PS} = 20$, 40, and 80%. The granules of PS 158K and LN3 were blended using a laboratory kneader Plasticorder PLE 651 (Brabender, Duisburg, Germany) with kneader barrels of type W50 HT at 200°C. The revolutions per minute were 70 min^{-1}, and the mixing time was $\sim$ 2 min. A nitrogen cover gas was used to protect the blend from thermo-oxidative degradation. The pure materials were also kneaded under the same conditions. The extrudates were dried in vacuum at $T = 50$°C for at least 18 h and compression molded at $T = 200$°C for 15 min into samples for shear and extensional rheology. The thickness of the cylindrical samples for the shear experiments was 2.0 mm, and their diameter was 22.0 mm. The samples for the melt extension experiments were cuboids of dimensions 1.5 $\times$ 7.0 $\times$ 56.0 mm^3. All samples were stored in vacuum until the rheological experiments were started.

Shear and extensional rheology

Linear viscoelastic shear oscillations were performed using the shear rheometer UDS 200 (Paar Physica, Stuttgart, Germany) at temperatures $T = 150$, 170, and 190°C. A plate-plate geometry was used, and the gap was set to 1.90 and 1.95 mm, respectively. Before each experiment, strain sweeps at two frequencies (ω = 0.5 $rads^{-1}$and ω = 50.0 $rads^{-1}$) were carried out to determine the range of linear viscoelastic deformations. In all experiments, the shear amplitude (γ_0 was set to $\gamma_0 = 0.01$. Finally, the data of the complex modulus at the different temperatures were shifted to the reference temperature $T_0 = 170$°C.

The uniaxial elongational rheometer RME was used for melt extension experiments which were followed by a relaxation and a recovery interval, respectively.[42] The test temperature was $T = 170$°C and the applied Hencky strain rate was $\dot{\varepsilon}_0 = 0.1\ s^{-1}$. Three different kinds of experiments were performed: (i) First, melt elongation tests with the constant strain rate $\dot{\varepsilon}_0$ = 0.1 s^{-1} up to different values of maximum Hencky strain ε_{max} were carried out. The values of ε_{max} were $\varepsilon_{max} = 1.5$ which corresponds to the stretch ratio $\lambda_{max} = 4.5$ and $\varepsilon_{max} = 3.0$ (equivalent to $\lambda_{max} = 20.1$). (ii) Second, melt elongation experiments up to ε_{max} = 3.0 and subsequent relaxation at constant strain for 10 min were performed. (iii) Recovery experiments after melt elongation to $\varepsilon_{max} = 3.0$ were also carried out. For these retardation experiments, a pair of scissors is installed in our RME.[43] In our experiments, the sample was elongated to the maximum Hencky strain ε_{max}. Immediately after the maximum strain ε_{max} had been attained, the scissors cut the stretched sample. Then the externally applied stress was zero and the sample which was still supported by the nitrogen cushion could recover freely. The transient recovery of the materials was determined by analysis of video sequences.

Morphology

To freeze in the morphology of elongated samples at different values of Hencky strain ε_{quench}, the chamber of the RME was opened $\sim$ 4 s before ε_{quench} was attained. Then a special cooling device was inserted into the RME, and the stretched sample was quenched at time $t = t_{quench} = \varepsilon_{quench}/\dot{\varepsilon}_0$ using liquid nitrogen. This procedure led to a rapid solidification of the sample.[44]

The morphology of the (i) undeformed, (ii) elongated, (iii) elongated and subsequently relaxed, and (iv) elongated and subsequently recovered samples was investigated by a transmission electron microscope (120 kV EFTEM LEO 912 Ω, LEO, Zeiss, Oberkochen, Germany). For these examinations ultrathin sections with a thickness less than 100 nm were prepared at room temperature from a small block of each specimen using a cryo-ultramicrotome (Leica, Wetzlar, Germany). The sections were treated with osmium tetroxide (OsO_4) vapor to stain selectively the polybutadiene (PB)-rich phase of the polymer. As a result, the PB-rich and the polystyrene (PS)-rich phases appear dark and bright in the TEM images, respectively.

RESULTS

Figure 2 presents the results of the linear viscoelastic shear oscillations which give insight into the relaxation behavior at small deformations. The storage modulus G' and the loss modulus G'' of polystyrene PS 158K attain a shape which is typical for polydisperse linear homopolymers and which can be reproduced by a multimode Maxwell model: At large frequencies (0.5 $rads^{-1} < \omega <$ 4000 $rads^{-1}$) the storage modulus is larger than the loss modulus and for the loss tangent $\tan\delta = G''/G' < 1$ holds, whereas at low frequencies the loss modulus exceeds the storage modulus, i.e., $\tan\delta > 1$. In the limit $\omega \to 0$, the Maxwell model leads to the power-laws $G' \propto \omega^2$ and $G'' \propto \omega$ which are not completely attained by the data in the frequency range of our measurements. The complex modulus of LN3 depicts a different frequency-dependent behavior. The storage and the loss

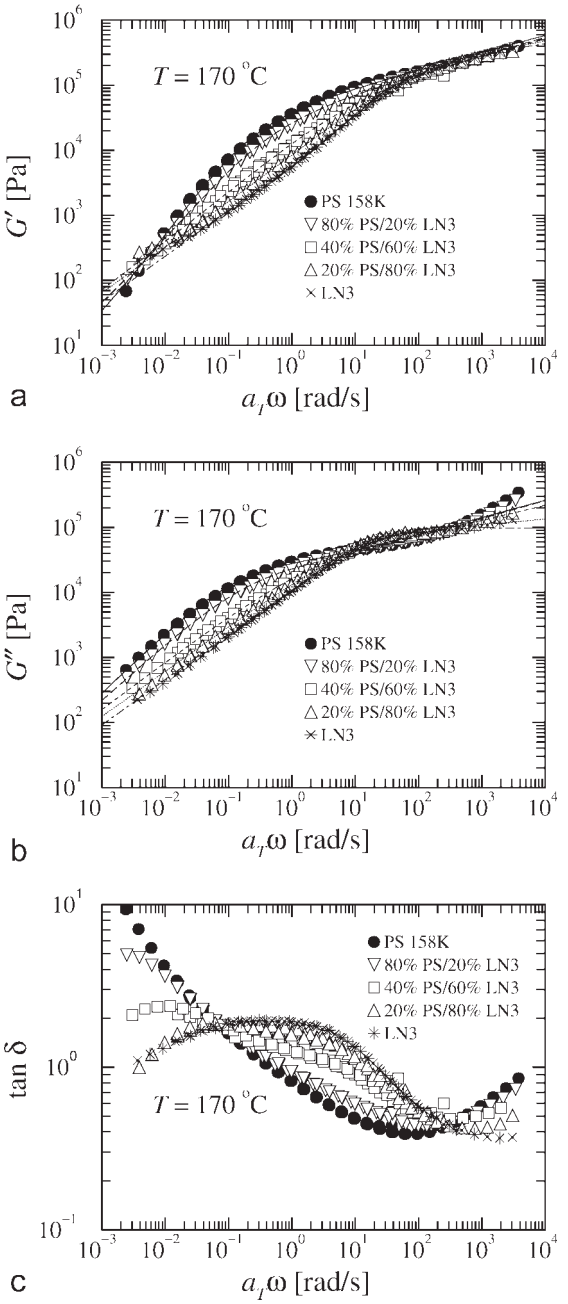

Figure 2 (a) Storage modulus G', (b) loss modulus G'', and (c) loss tangent $\tan \delta = G''/G'$ of PS 158K, LN3 and the three PS 158K/LN3 blends as a function of frequency ω at reference temperature $T_0 = 170°C$. The shift factor is denoted by a_T. The lines in (a) and (b) are the result of a nonlinear least-squares fit of eqs. (6) and (7) to the experimental data.

modulus of LN3 depict the scaling behavior $G' \propto \omega^{0.75}$ and $G'' \propto \omega^{0.68}$ in the range of moderate frequencies ($0.1 \text{ rads}^{-1} \leq \omega \leq 10.0 \text{ rads}^{-1}$). These power-laws moderately differ from the power-laws $G' \approx G'' \propto \omega^{1/2}$ which are generally observed for a lamellar morphology and are reproduced by the theory of Kawasaki and Onuki.[24] The storage modulus and the loss modulus of the three different PS 158K/LN3 blends attain values which vary monotonically with concentration of PS 158K between G' and G'' of the single components. At large frequencies, the dynamic moduli of PS 158K and LN3 do not differ much, and hence the blends attain similar G' and G'' values. At low frequencies, the complex modulus of the PS 158K/LN3 blends ranges between the corresponding values of neat PS 158K and LN3. The loss tangent $\tan \delta = G''/G'$ as a function of ω for the single components and the blends also displays this mixing effect, see Figure 2(c). The loss tangent of PS 158K depicts a minimum in the plateau region and then increases with decreasing ω, since viscous flow dominates at low frequencies. LN3 attains $\tan \delta$ values not far from unity with a maximum at $\omega \approx 0.3 \text{ rads}^{-1}$. The intermediate behavior of the blends is demonstrated by the less pronounced maximum of $\tan \delta$ with increasing PS 158K content.

The transient extensional viscosity $\mu(t)$ is given by

$$\mu(t) = \sigma(t)/\dot{\varepsilon}_0 \tag{1}$$

with the measured tensile stress $\sigma(t)$ and the applied Hencky strain rate $\dot{\varepsilon}_0$. Figure 3(a) presents $\mu(t)$ of PS 158K, LN3 and the three different blends. We plot both the measured data and in addition the linear viscoelastic prediction $\mu^0(t) = 3\eta^0(t)$ where $\eta^0(t)$ is the transient shear viscosity in the linear viscoelastic regime (vide infra). For LN3 we only plot the elongational viscosity for $t \leq 20$ s. The reason is that in our series of experiments it was impossible to stretch the pure LN3 homogeneously at larger times than 20 s, i.e., with a uniform cross section over the whole sample [cf. Fig. 3(b) for PS 158K]. In the very beginning of deformation, crumbling of the LN3 occurred, see Figure 3(c). The intensity of crumbling depended on the preparation procedure (processed using a kneader or not). It seems that the distribution of lamellar domains cannot be deformed such that the cross section of the sample is uniform all over the sample. On the other hand, in our experiments pure polystyrene and the three PS 158K/LN3 blends were homogeneously elongated in the molten state. In melt elongation, the transient extensional viscosity of PS 158K was much larger than the elongational viscosity $\mu(t)$ of LN3. At Hencky strain $\varepsilon = 1.5$, the viscosity ratio $p(\varepsilon)$ of PS 158K to LN3 roughly was $p(\varepsilon = 1.5) \approx 6.3$. The elongational viscosity of the three PS 158K/LN3 blends ranges between the curves of PS 158K and LN3. The elongational viscosity of the blend with 80% PS 158K did not differ much from $\mu(t)$ of neat PS 158K. With increasing weight fraction of LN3, the extensional viscosity of the blend deviates less from the curve of pure LN3. This behavior for the elongational viscosity is similar to the behavior of PS/PMMA blends where such a mixing effect was also observed.[43]

An additional interesting effect is depicted in Figure 4. In melt elongation experiments with the

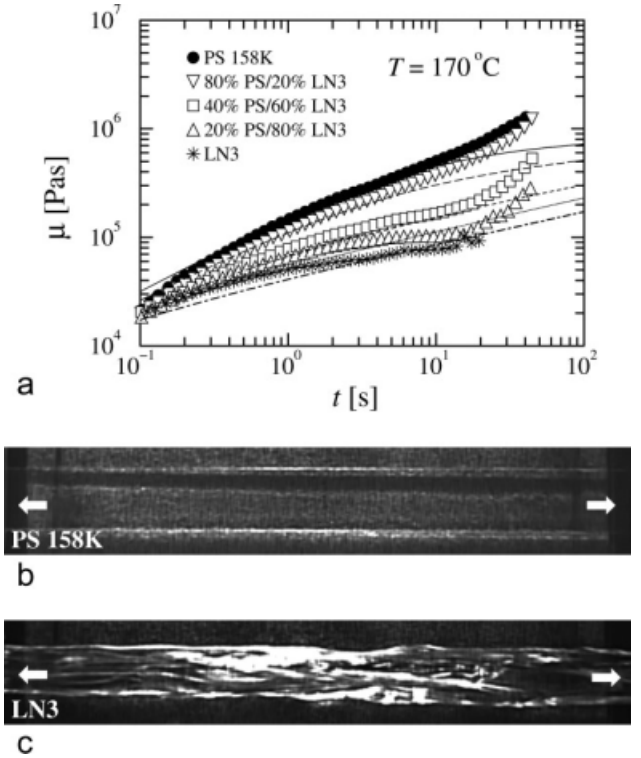

Figure 3 (a) Measured time-dependent elongational viscosity $\mu(t)$ (symbols) and the linear viscoelastic elongational viscosity $\mu_0(t)$ (lines, same order as experimental data) for PS 158K, LN 3 and the three PS 158K/LN3 blends. The test temperature was $T = 170°C$ and the Hencky strain rate $\dot{\varepsilon} = 0.1\ s^{-1}$. (b) Photograph of the PS 158K sample during melt elongation at Hencky strain $\varepsilon \approx 1.0$. (c) Photograph of the LN3 sample during melt elongation at $\varepsilon \approx 1.0$. The arrows indicate the direction of stretching.

RME,[42] samples with a rectangular cross section are used. Then the aspect ratio a_r of the cross section of the sample with width w_s and thickness t_s as a function of Hencky strain ε

$$a_r(\varepsilon) = w_s(\varepsilon)/t_s(\varepsilon) \tag{2}$$

generally remains constant during melt elongation, see $a_r(\varepsilon)$ for PS 158K (PS concentration 100%) in Figure 4. However for the three PS 158K/LN3 blends the value of a_r decreased with Hencky strain ε. This phenomenon was not observed for PS 158K and was more pronounced with increasing content of LN3. At $\varepsilon_{max} = 3.0$, the aspect ratio almost attained unity for the blends with 20 and 40% PS 158K. Finally, we emphasize that in spite of the dependence of the aspect ratio on strain, the area $A(\varepsilon)$ of the cross section was still in agreement with the incompressibility condition and decreased exponentially with Hencky strain ε, i.e., $A(\varepsilon) \propto \exp(-\varepsilon)$. Consequently, the stress of the elongated sample was correctly measured.

The transient recovered stretch λ_r (t')

$$\lambda_r(t') = L_{max}/L(t') \tag{3}$$

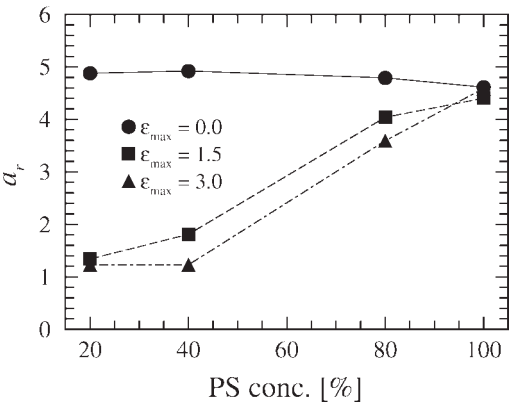

Figure 4 Aspect ratio $a_r = w_s/t_s$ of the cross section of the sample with width w_s and thickness t_s at different Hencky strains ε_{max}. The value for $\varepsilon_{max} = 0$ is the value of the compression molded sample.

is presented in Figure 5. Here, L_{max} is the length of the sample at cutting time $t = t_{max}$ and $L(t')$ the length of the sample at recovery time $t' = t - t_{max}$. In the initial stage of recovery, PS 158K recovered very rapidly. At large recovery times, λ_r of PS 158K still increased, but the slope of λ_r versus log t' decreased. At large t', the recoil of the polystyrene chains was terminated, but the surface tension of the sample caused an additional contribution to λ_r. Our investigations of the transient recovery of the crumbling LN3 revealed that the recoverable deformation of LN3 was less pronounced and much smaller than that of PS 158K, see Figure 5. In the initial stage of recovery, the λ_r values of the blends monotonically increased with concentration of the PS 158K phase. Interestingly, at roughly $t' = 200$ s the λ_r values of the 80% PS 158K/20% LN3 blend exceeded the corresponding λ_r values of PS 158K. This "overtaking" can be explained by an increase of

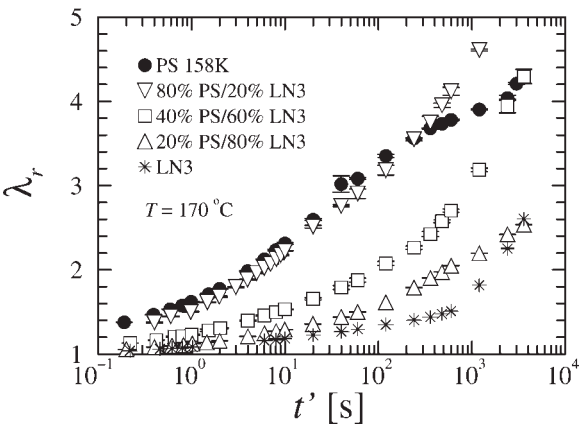

Figure 5 Transient recovered stretch λ_r as a function of recovery time t' for PS 158K and the three different PS 158K/LN3 blends. The Hencky strain rate was $\dot{\varepsilon}_0 = 0.1\ s^{-1}$, the maximum Hencky strain $\varepsilon_{max} = 3.0$ and the temperature $T = 170°C$. Note that LN3 could not be completely homogeneously extended.

the surface tension of the blend with increasing LN3 concentration and the lower viscosity of LN3 in comparison with PS 158K.

The morphology of the PS 158K/LN3 blends after compression molding and a residence time of 15 min in the RME is presented in Figure 6. After the molding and residence time, the morphology attained a quasi-equilibrium state and consisted of PS 158K and LN3 phases. The morphology of the blend with 80% PS 158K consisted of LN3 domains which were

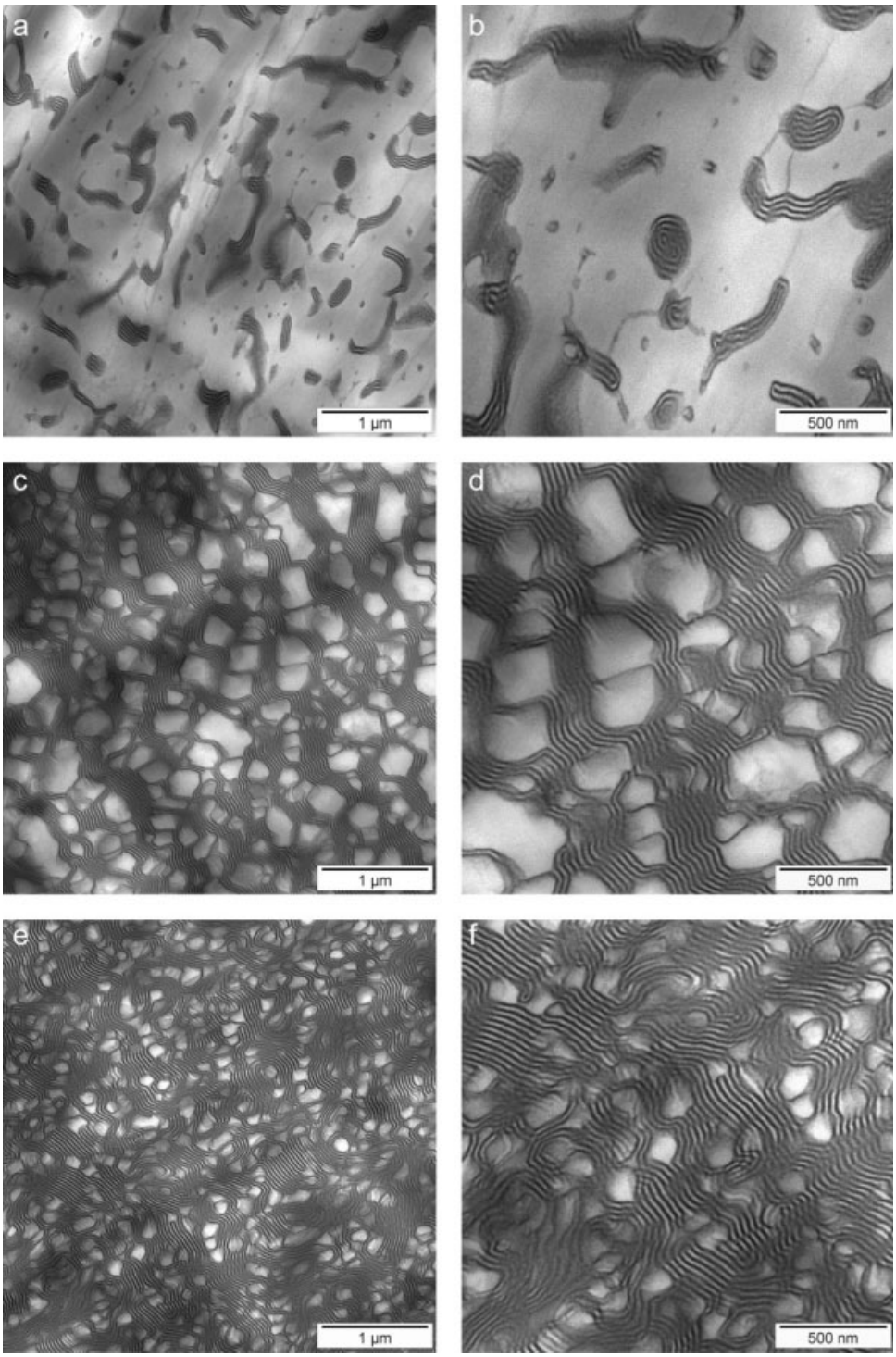

Figure 6 Transmission electron micrographs of the three PS 158K/LN3 blends after compression molding. The weight concentration of PS 158K is (a) and (b) 80%, (c) and (d) 40%, and (e) and (f) 20%. The micrographs depict a cross section of the sample perpendicular to the aluminum cover plates which were used for compression molding. In all micrographs, the polystyrene phase appears bright and the polybutadiene phase dark.

uniformly dispersed in the PS 158K matrix, see Figures 6(a,b). The LN3 domains themselves consisted of lamellae. Generally, these LN3 domains were not spherical which possibly resulted from compression molding. In addition, the LN3 domains did not recover to a spherical shape which indicates that the interfacial tension between the LN3 domains and the PS 158K matrix was very low. The LN3 domains typically comprised 6–11 lamellae, and their largest diameter ranged from ~300 to 1200 nm. Some of the LN3 domains attained a shape with a curved boundary. Figure 6(c,d) shows the morphology of the blend with 40% polystyrene. In this case, LN3 formed the continuous phase, and the PS 158K domains were uniformly dispersed in the LN3 matrix. The LN3 lamellae were aligned parallel to the aluminum cover plates which had been used for compression molding. Generally, the PS 158K inclusions were located in the PS lamellae and did not attain a fully circular shape. They attempted to splay as a PS lamella and went over into a PS lamellae in contrast to the solution-cast blends of Ref. 45. In doing so, the almost regularly spaced PS 158K inclusions attained a shape which reminds one to polygons. The typical size of the PS 158K inclusions was 300 nm. The morphology of the 20% PS 158K/80% LN3 blend was similar to the microstructure of the blend with 40% PS 158K, but the average size of the PS 158K domains, being in the order of 150 nm, was much smaller for the blend with 20% PS 158K than for the blend with 40% PS 158K. The PS 158K domains were also very homogeneously dispersed in the LN3 matrix for the blend with 20% PS 158K. For all three PS 158K/LN3 blends, the lamellae thickness did not depend on the PS 158K concentration and was approximately equal to 13 nm.

The three PS 158K/LN3 blends were extended with Hencky strain rate $\dot{\varepsilon}_0 = 0.1\ s^{-1}$ at $T = 170°C$ up to the maximum Hencky strain $\varepsilon_{max} = 3.0$. The morphology of the stretched blends is presented in Figure 7. The dispersed LN3 domains of the 80% PS 158K/20% LN3 blend were deformed into a needle-like shape. The deformed domains did not attain a smooth ellipsoidal shape which had been seen, e.g., for PS/PMMA blends,[43] but depicted a "rough" surface. The lamellar structure within the deformed LN3 phase was less clearly seen. For the two LN3-rich blends (the 40% PS 158K/60% LN3 and 20% PS 158K/80% LN3 blends) the alignment of the lamellae of the continuous LN3 phase parallel to the loading direction was increased, see also the melt extension experiments of Takahashi et al.[33] and Kobori et al.[35] In tensile experiments with LN3 in the solid state under uniaxial loading, the lamellae were also preferentially oriented parallel to the drawing direction.[40] In addition, the PS 158K inclusions were extended to the stretch ratio λ_d around 3.

After compression molding, the lamellae were oriented parallel to the aluminum cover plates. Figure 8 presents the flow-induced deformation of the morphology of the 20% PS 158K/80% LN3 blend after elongation to $\varepsilon_{max} = 1.5$ (corresponding to the stretch ratio $\lambda_{max} = 4.5$) and $\varepsilon_{max} = 3.0$ (i.e., at $\lambda_{max} = 20.1$). The strain rate was $\dot{\varepsilon}_0 = 0.1\ s^{-1}$ and the temperature $T = 170°C$. The micrographs reveal that the degree of alignment of the lamellae increased with applied maximum strain ε_{max}. In Figure 9, the morphology of the 40% PS 158/60% LN3 blend is presented for the elongation parameters $T = 170°C$, $\dot{\varepsilon}_0 = 0.1\ s^{-1}$ and $\varepsilon_{max} = 3.0$ after (a) subsequent relaxation (constant macroscopic strain) for 10 min and (b) after subsequent recovery (zero externally applied stress) for 60 min. The macroscopic extension of the blend led to an alignment of the lamellae. The lamellae of the LN3 matrix were still aligned parallel to the loading direction after the relaxation interval of 10 min ($t' = 600$ s),

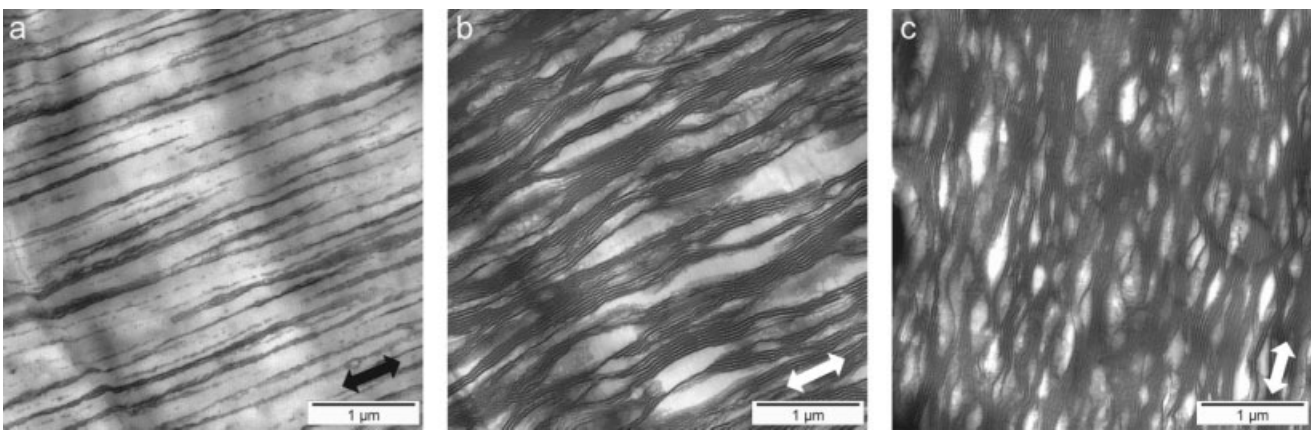

Figure 7 Transmission electron micrographs of the three PS 158K/LN3 blends after melt elongation at $T = 170°C$ to the maximum Hencky strain $\varepsilon_{max} = 3.0$ with Hencky strain rate $\dot{\varepsilon}_0 = 0.1\ s^{-1}$. The weight concentration of PS 158K is (a) 80%, (b) 40%, and (c) 20%. The arrow indicates the stretching direction.

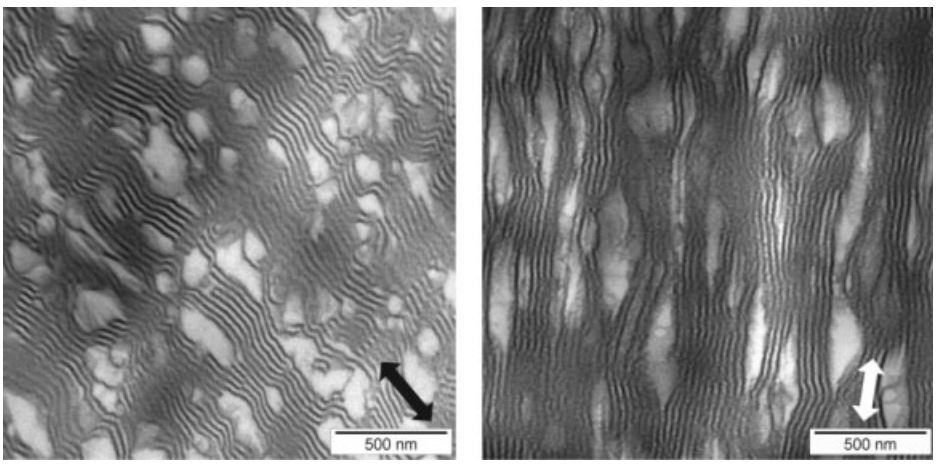

Figure 8 Transmission electron micrographs of the 20% PS 158K/80% LN3 blend which was elongated and subsequently quenched at $T = 170°C$ with Hencky strain rate $\dot{\varepsilon}_0 = 0.1\ s^{-1}$. The maximum Hencky strain was (a) $\varepsilon_{max} = 1.5$ and (b) $\varepsilon_{max} = 3.0$. The arrow indicates the stretching direction.

see Figure 9(a). In relaxation, the polymer chains of the PS 158K domains could recoil to an isotropic shape. During this process, the PS 158K chains partially deformed the neighbored lamellae, and therefore irregular undulations of the lamellae can be seen in Figure 9(a). The undulations of the lamellae of the 40% PS 158K/60% LN3 blend were mostly pronounced if the number of the lamellae between the inclusions was small. Figure 9(b) presents the morphology of the 40% PS 158K/60% LN3 blend after extension to $\varepsilon_{max} = 3.0$ and subsequent recovery for 60 min. In recovery after melt extension, the polymer chains of the PS 158K inclusions also recoiled to an isotropic state. During their recoil, the PS 158K chains caused a deformation of the LN3 matrix. Then the PS 158K domains were not stretched anymore and the alignment of the lamellae also decreased, see Figure 9(b).

Finally, in Figure 10 we present the morphology of the 80% PS 158K/20% LN 3 blend at relaxation time $t' = 10$ min. During relaxation, the filament-like LN3 domains of the 80% PS 158K/20% LN 3 blend slightly retracted and seemed to be twisted. This deformation of the LN3 domains was possibly caused by the relaxing PS 158K and LN3 chains. Since the extended LN3 domains only slightly retracted, it seems that the block copolymer chains were only moderately stretched during melt extension.

DISCUSSION

The linear viscoelastic behavior of PS 158K can be described by a multimode Maxwell model. In contrast to PS 158K, the pure LN3 depicts the power-laws $G' \propto \omega^{0.75}$ and $G'' \propto \omega^{0.68}$ in a certain frequency range. Such a behavior is not characteristic

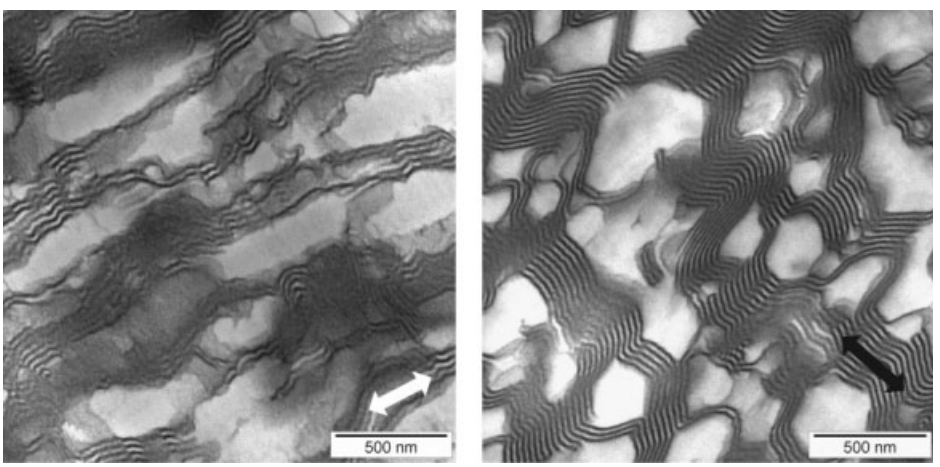

Figure 9 Transmission electron micrographs of the 40% PS 158K/60% LN3 blend after (a) relaxation for 10 min and (b) recovery for 60 min. The elongation parameters were $\dot{\varepsilon}_0 = 0.1\ s^{-1}$, $\varepsilon_{max} = 3.0$, and $T = 170°C$ (arrow = stretching direction).

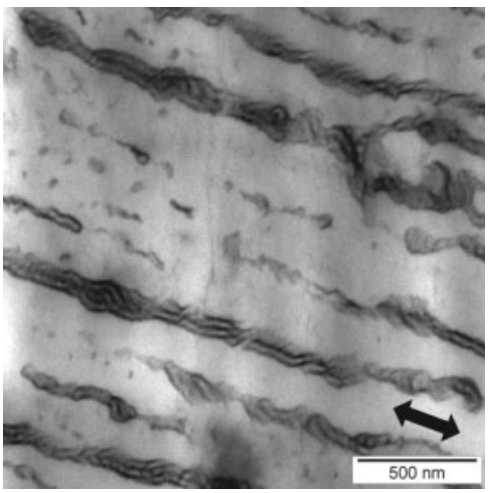

Figure 10 Transmission electron micrograph of the 80% PS 158K/20% LN3 blend after elongation with strain rate $\dot{\varepsilon}_0 = 0.1\ s^{-1}$ to the maximum Hencky strain $\varepsilon_{max} = 3.0$ at temperature $T = 170°C$ and subsequent relaxation for 10 min (arrow = stretching direction).

for a Maxwell model with a spring and a dashpot in series. To describe the linear viscoelastic response of PS 158K, LN3 and the blends using a single model, we apply the fractional Maxwell model which consists of two fractional elements in series, see Figure 11. The constitutive equation of each fractional element (depicted by a triangle) is given by

$$\sigma_{xy} = G_0 \tau_0^{\beta_i} d^{\beta_i} \gamma / dt^{\beta_i} \quad (4)$$

with the time-dependent shear stress $\sigma_{xy}(t)$ and the shear strain $\gamma(t)$ as well as the parameters τ_0 and β_i ($i = 1, 2$). Such kind of models and analogous hierarchical and fractal arrangements of springs and dashpots were studied in Refs. 46–48. In addition, a similar approach using the fractional Zener model was also successfully applied in Ref. 49. The parameters of the fractional Maxwell model are the elastic modulus G_0, the characteristic time τ_0, and the fractional exponents β_1 and β_2. Then the complex modulus $G^* = G' + iG''$ of the fractional Maxwell model as a function of frequency ω is given by

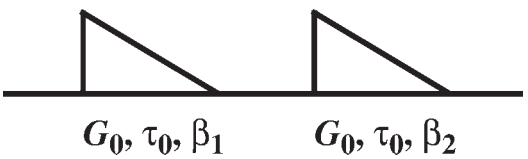

Figure 11 The fractional Maxwell model which consists of two fractional elements (depicted by the triangles) in series. The model parameters are the elastic modulus G_0, the characteristic time τ_0 and the fractional exponents β_1 and β_2. The constitutive equation of each fractional element ($i = 1, 2$) is given by $\sigma_{xy} = G_0\ \tau_{0i}^{\beta}\ d^{\beta_i}\ \gamma / dt^{\beta_i}$ with the shear stress $\sigma_{xy}(t)$ and the shear strain $\gamma(t)$ at time t.

$$G^*(\omega) = \frac{G_0 (i\omega\tau_0)^{\beta}}{1 + (i\omega\tau_0)^{\alpha}} \quad (5)$$

with the real and the imaginary parts G' and G''

$$G'(y) = G_0 y^{\beta} \frac{\cos(\beta\pi/2) + y^{\alpha}\ \cos[(\beta - \alpha)\pi/2]}{1 + 2y^{\alpha}\ \cos(\alpha\pi/2) + y^{2\alpha}} \quad (6)$$

$$G''(y) = G_0 y^{\beta} \frac{\sin(\beta\pi/2) + y^{\alpha}\ \sin[(\beta - \alpha)\pi/2]}{1 + 2y^{\alpha}\ \cos(\alpha\pi/2) + y^{2\alpha}} \quad (7)$$

In eqs. (5)–(7) the relations $y = \omega\tau_0$, $\alpha = \beta_1 - \beta_2 > 0$ and $\beta = \beta_1$ hold. The parameters α and β can attain values between 0 and 1. Then the transient shear viscosity $\eta^0(t)$ in the linear viscoelastic regime is given by[50]

$$\eta^0(t) = G_0 \tau_0 (t/\tau_0)^{1+\alpha-\beta} E_{\alpha,2+\alpha-\beta}[-(t/\tau_0)^{\alpha}] \quad (8)$$

where $E_{\kappa,v}[x] = \sum_{n=0}^{\infty} x^n / [\Gamma(n\kappa + v)]$ is the generalized Mittag-Leffler function and $\Gamma(x)$ the Gamma function. Finally, the linear viscoelastic prediction $\mu^0(t)$ of the transient elongational viscosity in simple elongation follows from $\mu^0(t) = 3\eta^0(t)$.

The functions $G'(\omega)$ and $G''(\omega)$ of eqs. (6) and (7) were fitted to the experimental data for the neat blend components and the three PS 158K/LN3 blends. The results of the fits are shown in Table II and Figure 2. The complex modulus $G^*(\omega)$ of the fractional Maxwell model reproduces very well the experimental data for the pure blend components and the three PS 158K/LN3 blends. Using the fit parameters α, β, G_0, and τ_0, the elongational viscosity $\mu^0(t) = 3\eta^0(t)$ in the linear viscoelastic regime [see Eq. (8)] was calculated and plotted in Figure 3. At small times ($t \leq 2$ s), the measured elongational viscosity $\mu(t)$ of all materials nearly agrees with the linear viscoelastic prediction $\mu^0(t)$. The agreement is best for PS 158K and moderate for the 20% PS 158K/80% LN 3 blend. At larger times, the extensional viscosity $\mu(t)$ exceeds the linear viscoelastic prediction $\mu^0(t)$ for PS 158K and the three blends. This effect is denoted by strain-hardening.

The crumbling of LN3 during our melt elongation experiments is an unusual effect, see Figure 3(c). A possible explanation of this crumbling phenomenon can be given by taking into account the nearly

TABLE II
Results of the Nonlinear Least-Squares Fit of Equations (6) and (7) to the Experimental G′(ω) and G″(ω) Data

	α	β	G_0 (Pa)	τ_0 (s)
PS 158K	0.6732	0.9410	32969	6.4766
80% PS 158K/20% LN3	0.6054	0.8865	30846	3.9213
40% PS 158K/60% LN3	0.4903	0.7372	83272	0.2338
20% PS 158K/80% LN3	0.5429	0.6965	216421	0.0263
LN3	0.5869	0.7000	263694	0.0135

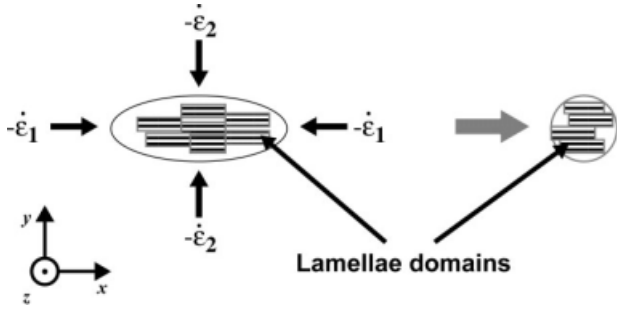

Figure 12 Schematic presentation of the deformation of neighbored domains of lamellae during elongation of LN3. The loading direction is parallel to the z axis. The figure presents a cross section of the sample perpendicular to the loading direction. The thickness of the lamellae is not decreased by the compressive flow, but the domains rearrange.

constant thickness of the lamellae. The thickness of the lamellae does not vary much with applied extensional strain ε_{max}. Therefore, as a first approximation, the thickness of the lamellae can be considered as constant. Because of the macroscopic deformation of the sample, a compressive flow perpendicular to the loading direction exists which would lead to the strain rate $\dot{\varepsilon}_0/2$ perpendicular to the loading direction for an isotropic fluid. Since the thickness of the lamellae is almost constant and the lamellae do not seem to be compressible, the lamellar domains rearrange by keeping the thickness of the lamellae constant, see Figure 12. Macroscopically, this rearrangement is associated with a crumbling of the sample. In the PS 158K/LN3 blends, the PS 158K inclusions behave like an isotropic viscoelastic fluid. During extension of the blends, the lamellar domains also rearrange by keeping the thickness of the lamellae constant. This effect leads to a nonradial velocity component perpendicular to the loading direction and thus to an anisotropic Poisson ratio. Consequently, the width and the thickness of the cross section of the blends do not decay proportional to $\exp(-\varepsilon/2) = \lambda^{-1/2}$ for the blends. On the contrary, the aspect ratio $a_r(\varepsilon)$ decreased with Hencky strain ε, see Figure 4. Crumbling is not observed for the blends, since the PS 158K inclusions can balance the rearrangement of the lamellar domains so that a macroscopic uniform cross section is achieved.

CONCLUSIONS

We studied the rheological properties and the flow-induced changes of the morphology of blends of a general purpose polystyrene (PS 158K) and a styrene-butadiene block copolymer (LN3). Our linear viscoelastic shear oscillations and melt extension experiments revealed that the rheological properties of blends of polystyrene and a block copolymer result from a mixing effect of the properties of the single components. The data of the complex modulus as a function of angular frequency in the flow regime can be well reproduced by the fractional Maxwell model for all materials. In our melt elongation experiments, the block copolymer LN3 could not be extended with a constant cross section over the whole sample for our set of parameters. On the contrary, the specimens started to crumple at a small Hencky strain. This effect was caused by the nearly constant thickness of the lamellae during elongation. Instead of being strongly stretched, the lamellar domains rearranged during melt elongation, and their alignment was more pronounced. The presence of the PS 158K domains in the PS 158K/LN3 blends led to a macroscopically more uniform elongation. Our morphological investigations revealed that the domains of the disperse phase (PS 158K inclusions in the LN3 matrix resp. LN3 domains in the PS 158K matrix) were extended in elongational flows. Melt elongation of the LN3-rich blends led to an increase of the alignment of the lamellae of the LN3 matrix parallel to the loading direction. The thickness of the lamellae did not change very much during elongation. In subsequent relaxation, the alignment of the LN3 lamellae still persisted, whereas the PS 158K macromolecules recoiled. This recoil of the PS 158K chains caused a partial deformation of the lamellae. In recovery after melt extension, the alignment of the lamellae parallel to the loading direction decreased.

The authors thank Prof. J. Meissner and Prof. H.C. Öttinger for their valuable discussions, and Prof H.-J. Radusch and Dr. L. Fiedler (both MLU Halle-Wittenberg) for providing of the internal mixer. They also thank C. Becker, S. Scholtyssek, V. Seydewitz (all MLU Halle-Wittenberg), F. Mettler, and W. Schmidheiny (both ETH Zurich) for their support of the experiments.

References

1. Folkes, M. J., Ed. Processing, Structure and Properties of Block Copolymers; Elsevier Applied Science Publishers: London, 1985.
2. Hamley, I. W. The Physics of Block Copolymers; Oxford University Press: Oxford, 1998.
3. Lodge, T. P. Macromol Chem Phys 2003, 204, 265.
4. Leibler, L. Prog Polym Sci 2005, 30, 898.
5. Ruzette, A.-V.; Leibler, L. Nat Mater 2005, 4, 19.
6. Knoll, K.; Niessner, N. Macromol Symp 1998, 132, 231.
7. Aggarwal, S. L.; Livigni, R. A. Polym Eng Sci 1977, 17, 498.
8. Ivankova, E. M.; Adhikari, R.; Michler, G. H.; Weidisch, R.; Knoll, K. J Polym Sci Part B: Polym Phys 2003, 41, 1157.
9. Michler, G. H.; Adhikari, R.; Henning, S. J Mater Sci 2004, 39, 3281.
10. Satapathy, B. K.; Lach, R.; Weidisch, R.; Schneider, K.; Janke, A.; Knoll, K. Eng Fract Mech 2006, 73, 2399.
11. Adhikari, R.; Michler, G. H. Prog Polym Sci 2004, 29, 949.
12. Fredrickson, G. H. J Chem Phys 1986, 85, 5306.
13. Fredrickson, G. H.; Helfand, E. J Chem Phys 1988, 89, 5890.

14. Rosedale, J. H.; Bates, F. S. Macromolecules 1990, 23, 2329.
15. Larson, R. G.; Winey, K. I.; Patel, S. S.; Watanabe, H.; Bruinsma, R. Rheol Acta 1993, 32, 245.
16. Polis, D. L.; Winey, K. I.; Ryan, A. J.; Smith, S. D. Phys Rev Lett 1999, 83, 2861.
17. Qiao, L.; Winey, K. I. Macromolecules 2000, 33, 851.
18. Qiao, L.; Winey, K. I.; Morse, D. C. Macromolecules 2001, 34, 7858.
19. Mandare, P.; Winter, H. H. Rheol Acta 2007, 46, 1161.
20. Winter, H. H.; Scott, D. B.; Gronski, W.; Okamoto, S.; Hashimoto, T. Macromolecules 1993, 26, 7236.
21. Chen, Z.-R.; Kornfield, J. A. Polymer 1998, 39, 4679.
22. Chung, C. I.; Gale, J. C. J Polym Sci Polym Phys 1976, 14, 1149.
23. Gupta, V. K.; Krishnamoorti, R.; Kornfield, J. A.; Smith, S. D. Macromolecules 1995, 28, 4464.
24. Kawasaki, K.; Onuki, A. Phys Rev A 1990, 42, 3664.
25. Qiao, L.; Ryan, A. J.; Winey, K. I. Macromolecules 2002, 35, 3596.
26. Thunga, M.; Staudinger, U.; Satapathy, B. K.; Weidisch, R.; Abdel-Goad, M.; Janke, A.; Knoll, K. J Polym Sci Part B: Polym Phys 2006, 44, 2776.
27. Geiger, K.; Knoll, K.; Langela, M. Rheol Acta 2002, 41, 345.
28. Leist, H.; Geiger, K.; Wiesner, U. Macromolecules 1999, 32, 1315.
29. Carreras, E. S.; Piau, J.-M.; El Kissi, N.; Pignon, F.; Panine, P. J Rheol 2006, 50, 803.
30. Phatak, A.; Macosko, C. W.; Bates, F. S.; Hahn, S. F. J Rheol 2005, 49, 197.
31. Langela, M.; Wiesner, U.; Spiess, H. W.; Wilhelm, M. Macromolecules 2002, 35, 3198.
32. Stangler, S.; Abetz, V. Rheol Acta 2003, 42, 569.
33. Takahashi, T.; Toda, H.; Minagawa, K.; Takimoto, J.-I.; Iwakura, K.; Koyama, K. J Appl Polym Sci 1995, 56, 411.
34. Kotaka, T.; Okamoto, M.; Kojima, A.; Kwon, Y. K.; Nojima, S. Polymer 2001, 42, 1207.
35. Kobori, Y.; Kwon, Y. K.; Okamoto, M.; Kotaka, T. Macromolecules 2003, 36, 1656.
36. Lee, W.-K.; Kim, H. D.; Kim, E. Y. Curr Appl Phys 2006, 6, 718.
37. Nojima, S.; Roe, R.-J. Macromolecules 1987, 20, 1866.
38. Buschnakowski, M.; Adhikari, R.; Michler, G. H.; Knoll, K. J Appl Polym Sci 2007, 106, 1939.
39. Antony, P.; Puskas, J. E.; Kontopoulou, M. Polym Eng Sci 2003, 43, 243.
40. Adhikari, R.; Huy, T. A.; Buschnakowski, M.; Michler, G. H.; Knoll, K. New J Phys 2004, 6, 28.
41. Gramespacher, H.; Meissner, J. J Rheol 1997, 41, 27.
42. Meissner, J.; Hostettler, J. Rheol Acta 1994, 33, 1.
43. Handge, U. A.; Pötschke, P. J Rheol 2004, 48, 1103; Erratum: J Rheol 2005, 49, 1553.
44. Handge, U. A.; Schmidheiny, W. Rheol Acta 2007, 46, 913.
45. Huy, T. A.; Adhikari, R.; Lüpke, T.; Michler, G. H.; Knoll, K. Polym Eng Sci 2004, 44, 1534.
46. Schiessel, H.; Blumen, A. J Phys A Math Gen 1993, 26, 5057.
47. Heymans, N.; Bauwens, J.-C. Rheol Acta 1994, 33, 210.
48. Friedrich, C. J Non-Newtonian Fluid Mech 1993, 46, 307.
49. Sailer, C.; Handge, U. A. Macromolecules 2007, 40, 2019.
50. Friedrich, C.; Braun, H. Rheol Acta 1992, 31, 309.